SUPPLEMENTARY MATERIAL
Multifunctional magnonic platform based on the interplay between spin-wave waveguide and nanodots with PMA and DMI

Krzysztof Szulc,[1, 2, a)] Mateusz Zelent,[2] and Maciej Krawczyk[2]
[1)] *Institute of Molecular Physics, Polish Academy of Sciences, M. Smoluchowskiego 17, 60-179, Poznań, Poland*
[2)] *Institute of Spintronics and Quantum Information, Faculty of Physics and Astronomy, Adam Mickiewicz University, Uniwersytetu Poznańskiego 2, 61-614, Poznań, Poland*

(Dated: 14 August 2025)

Materials with perpendicular magnetic anisotropy (PMA) and antisymmetric exchange interactions are widely explored in spintronics but are of limited use in magnonics due to high damping. We present a hybrid magnonic crystal composed of a chain of circular nanodots with strong PMA and Dzyaloshinskii–Moriya interaction (DMI), positioned above a spin-wave waveguide made of permalloy. Due to the dipolar coupling between the subsystems, a strongly bound hybrid magnetization texture is formed, with two stable magnetization states in the nanodots: a single-domain state and an egg-shaped skyrmion state, allowing reprogramming of the system properties. Numerical results show complex spin-wave spectra with several key features for magnonics: programmable Bragg and non-Bragg band gaps correlated with magnon–magnon couplings, the flat bands and bound states for the skyrmion state, and exclusively waveguide-dominated modes for the single-domain state. With these properties, the proposed hybrid magnonic crystal has different functionalities that overcome the damping limitations of materials with PMA and DMI and open up potential applications in spin-wave filtering, spin-wave generation, quantum magnonics, and analog magnonics, in particular in the realization of magnonic neural networks.

S1. DESCRIPTION OF MODE LOCALIZATION

The parameter of the mode localization introduced in Eq. 3 and shown in Fig. 4(a-d) and its connection with the mode profiles shown in Fig. 4(e) are not straightforward. In this section, we extend the description of mode localization basing on two hybridized branches—one dot-dominated and second waveguide-dominated—at around 5.6 GHz in the W/Sk system. They are shown in Fig. S1. Figs. S1(a-b) show the zoom-in of Figs. 4(c-d) from the manuscript. From the bottom of these two branches, we have chosen 5 modes of different wavevector with different values of localization. Their mode profiles are shown in Fig. S1(c).

The top row of Fig. S1(c) shows the m_y component of the magnetization, the same as in Fig. 4(e). In the bottom row, the spatial distribution of the $|\mathbf{m}|^2$ is shown. This value is under the integral in Eq. 4, which is used to calculate the mode localization, therefore, assuming almost uniform distribution of $\mathbf{m}$ across the thickness of the dot and waveguide, these graphs are graphical representations of mode localization. This is apparent from the comparison of the top and bottom row of Fig. S1(c) that the distribution of m_y is not equivalent to $|\mathbf{m}|^2$. The area of the distribution of both parameters matches for the waveguide but it is different for dot as the nodal line for m_y component along the skyrmion circumference matches the maximum of $|\mathbf{m}|^2$. Also, the relative amplitude is different, e.g., while m_y distribution of the mode M-3 gives similar maximum values, for $|\mathbf{m}|^2$ distribution the maximum is significantly higher in the dot. It is because of the difference in the contribution of each magnetization component to the mode localization. In the waveguide, the m_y component shown in the mode profiles is strongly dominant. In the dot in skyrmion state, the highest amplitude component is m_z, but is less dominant than m_y component in the waveguide. Because of this, the distributions of m_y and $|\mathbf{m}|^2$ matches only to some extent. It is also worth to look more careful on the distribution of $|\mathbf{m}|^2$. The mode M-3 has the localization close to 0.5 – the situation where it is equally distributed between the dot and the waveguide. Despite that, the maximum amplitude is significantly larger in the dot. One can notice that the amplitude in the dot is distributed over smaller area than in the waveguide but, except of that, the contribution of the thickness should not be forgotten—the thickness of the waveguide is three times larger than of the dot, so the total intensity of a cross-section should be approximately three times smaller in the waveguide to lead to mode localization of 0.5.

S2. THE DYNAMICS OF ISOLATED SUBSYSTEMS

Figure S2(a) shows the comparison between the dynamics of the isolated subsystems. The dispersion relation of an isolated waveguide is shown with solid blue lines. The resonant modes of a dot are shown with horizontal dashed lines: orange line for an isolated dot in the single-domain state and green line for an isolated dot in the skyrmion state.

The lowest zero-k frequency of the waveguide is 4.04 GHz and it reaches a minimum of 3.76 GHz for $k = 9.0\,\mathrm{rad}/\mu\mathrm{m}$. Higher-order modes have their minima at 6.19 GHz, 8.17 GHz, 9.92 GHz, and 11.57 GHz, respectively. First four modes exhibit a backward-wave regime at small wavevectors, while higher modes can only propagate forward.

[a)] Electronic mail: szulc@ifmpan.poznan.pl

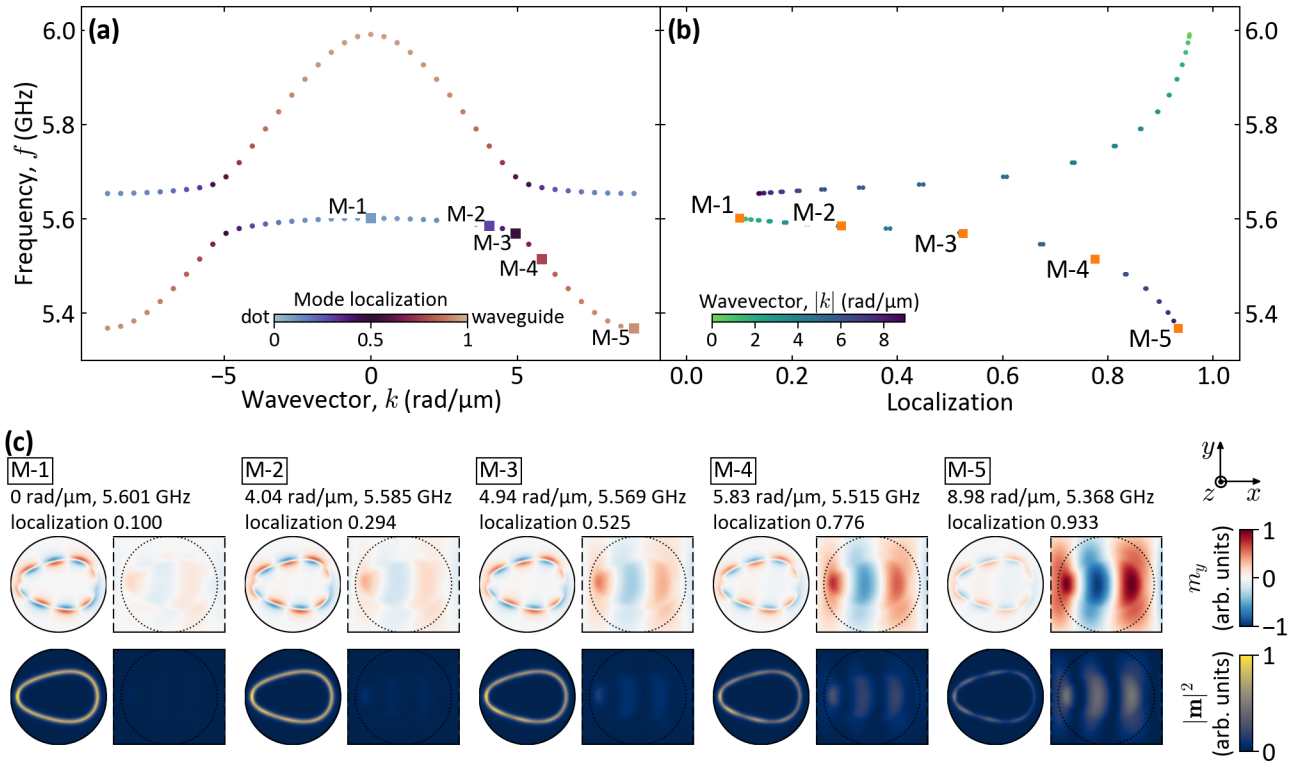

FIG. S1. (a-b) The zoom-in of Figures 4(c-d) showing the dispersion relation in the first Brillouin zone and localization in the W/Sk system. (c) The SW mode profiles for 5 modes marked from M-1 to M-5 in (a) and (b). The modes are marked on the dispersion relations with a square point and a label. In the top row, each mode profile displays the m_y magnetization component in the xy-plane at the center of the dot (left side) and at the center of the waveguide (right side). The intensity is normalized so that the maximum value of $|m_y|$ is 1 for each of the mode profiles. In the bottom row, analogically, the local intensity is shown calculated as $|\mathbf{m}|^2$.

In case of the dot, its static configuration has a very large impact on the frequency of resonant modes. In a single-domain state, the lowest mode has a frequency of 8.89 GHz and it is a fundamental mode (SD-1). Modes with higher frequencies are clockwise (CW) [e.g. SD-2] and counterclockwise (CCW) [e.g. SD-3] azimuthal modes, as well as higher-order radial modes (e.g. SD-4).

The skyrmion state exhibits numerous low-frequency modes, which are all CW (e.g. Sk-1) and CCW (e.g. Sk-3) azimuthal modes in the skyrmion domain wall, except of one skyrmion breathing mode (Sk-2) (which can be considered the 0th order azimuthal mode). The first mode not associated with the skyrmion domain wall is the fundamental mode of a skyrmion core (Sk-4) at the frequency 9.47 GHz. The higher-frequency modes includes higher-order azimuthal and radial modes, which can be localized either in the skyrmion core (e.g. Sk-5), outside the skyrmion (e.g. Sk-7) or in both the core and outside (e.g. Sk-6). Interestingly, some of the skyrmion domain wall modes in this range can also be strongly excited outside the skyrmion (e.g. Sk-8).

S3. COMPARISON BETWEEN W/SK SYSTEM AND A DOT CHAIN

In order to investigate the contribution of the dipolar interaction between the dot and the waveguide to the bandwidth of the skyrmion domain wall modes, we studied a one-dimensional chain of dots in skyrmion state, which is a subsystem of the W/Sk system. Additionally, as a reference, we studied a single dot in a skyrmion state.

Table S1 shows the simulation data for the modes within the frequency range I of the W/Sk system, as depicted in Fig. 4(c,d) in the main manuscript. This range contains 15 modes, ranging from the 2nd CW to the 12th CCW mode. Modes at higher frequencies may be significantly impacted by interaction with waveguide modes and are therefore not included in Table S1.

First of all, it is important to note that the static configurations of these systems are different. In a single dot, the skyrmion is round. In a dot chain, the dipolar interaction between the dots is very small so the skyrmion remains round. In the W/Sk system, the skyrmion changes its shape to an egg-like shape, as shown in Fig. 2(c) in the main manuscript. This change in shape significantly impacts the mode frequencies. As shown in Table S1, the frequencies of modes in a single dot and an array of dots are very similar, differing by no more

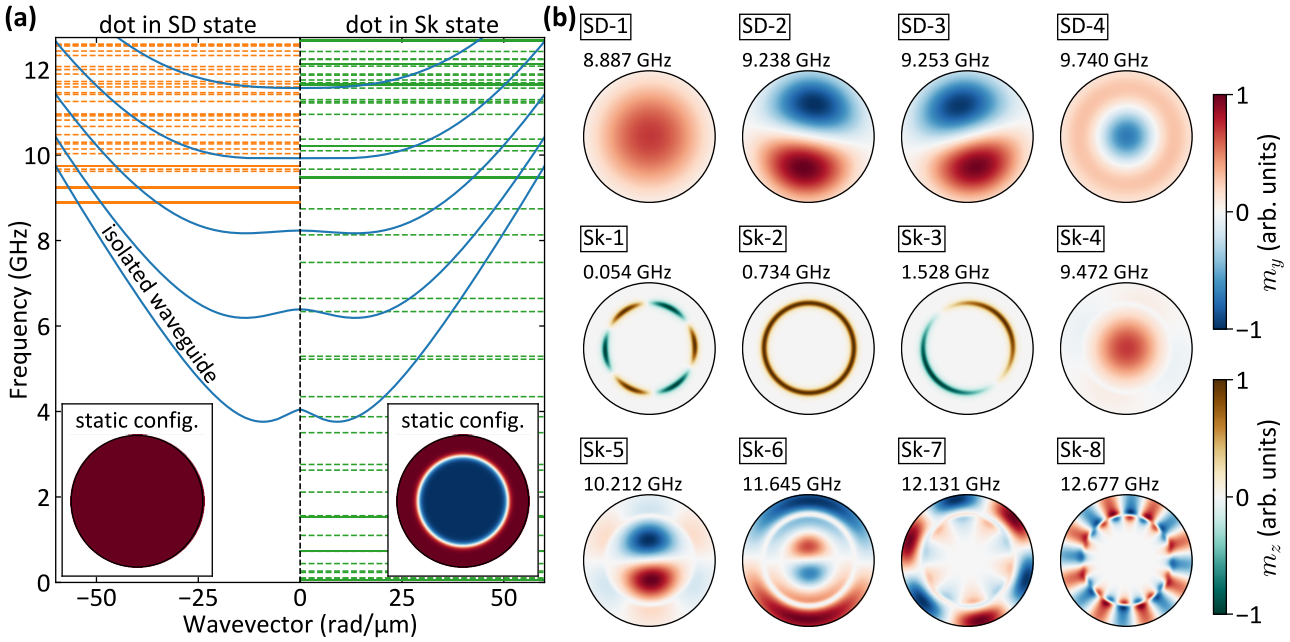

FIG. S2. (a) Dispersion relation of an isolated waveguide (solid blue lines) and frequencies of the resonant modes of a dot in a single-domain state (horizontal dashed orange lines) and in a skyrmion state (horizontal dashed green lines). Solid orange and green lines correspond to the modes which profiles are shown in (b). Please note that the resonant modes are characterized solely by their frequencies and they are not connected with the wavevector presented on the horizontal axis. The division of the single-domain state and skyrmion modes on the negative and positive wavevector sides is made solely for the sake of presentation clarity. (b) Resonant mode profiles of the dot of four modes in the SD state and eight modes in the Sk state. Please note that all SD modes and Sk-4 – Sk-8 modes are presented with m_y component (top color bar), while modes Sk-1 – Sk-3 are presented with m_z component (bottom color bar). All modes are normalized to the maximum absolute value of the mode. The animated version of this figure is available in Supplementary Material.

TABLE S1. The comparison of the skyrmion domain wall modes in three different systems: single dot, dot chain, and W/Sk system as defined in the main manuscript. For a single dot, we present the value of the mode frequency, while for dot chain and W/Sk system, we show the lowest and the highest frequency of the band and the bandwidth. Please note that the frequencies are in MHz, while bandwidths are in kHz.

	Single dot	Dot chain			W/Sk system		
Mode	f (MHz)	$f_{\min}$ (MHz)	$f_{\max}$ (MHz)	Bandwidth (kHz)	$f_{\min}$ (MHz)	$f_{\max}$ (MHz)	Bandwidth (kHz)
CW 2	2628	2627	2628	1309.06	3065	3078	13085.05
CW 1	1528	1542	1549	7533.08	2023	2044	21187.33
breathing	734	747	780	33223.62	1192	1226	34143.46
CCW 1	266	290	296	5996.20	482	490	8453.12
CCW 2	91	106	107	354.05	238	239	1061.96
CCW 3	54	64	64	42.51	107	108	533.27
CCW 4	106	117	117	264.79	132	133	178.41
CCW 5	235	237	237	13.78	303	304	728.22
CCW 6	441	438	438	2.25	505	505	208.15
CCW 7	729	719	719	1.99	780	781	265.48
CCW 8	1101	1083	1083	0.96	1140	1140	26.74
CCW 9	1561	1534	1534	8.47	1586	1586	36.19
CCW 10	2113	2075	2075	0.10	2122	2122	9.06
CCW 11	2760	2710	2710	0.08	2750	2750	11.54
CCW 12	3504	3440	3440	0.01	3474	3474	54.62

than 65 MHz. On the other hand, modes in the W/Sk system can differ from a single dot modes as much as 516 MHz for the 1st CW mode. However, for the higher-order CCW modes, this difference is strongly reduced.

When comparing the bandwidths of the same modes in different systems, it is clear that the dipolar interaction between the dot and the waveguide significantly contributes to this value. The bandwidths of all modes, except of the 4th CCW mode, are larger in W/Sk system, indicating that the presence of the waveguide enhance the interaction between the skyrmions. This effect is particularly noticeable for higher-order CCW modes (5th order and higher), whose bandwidths

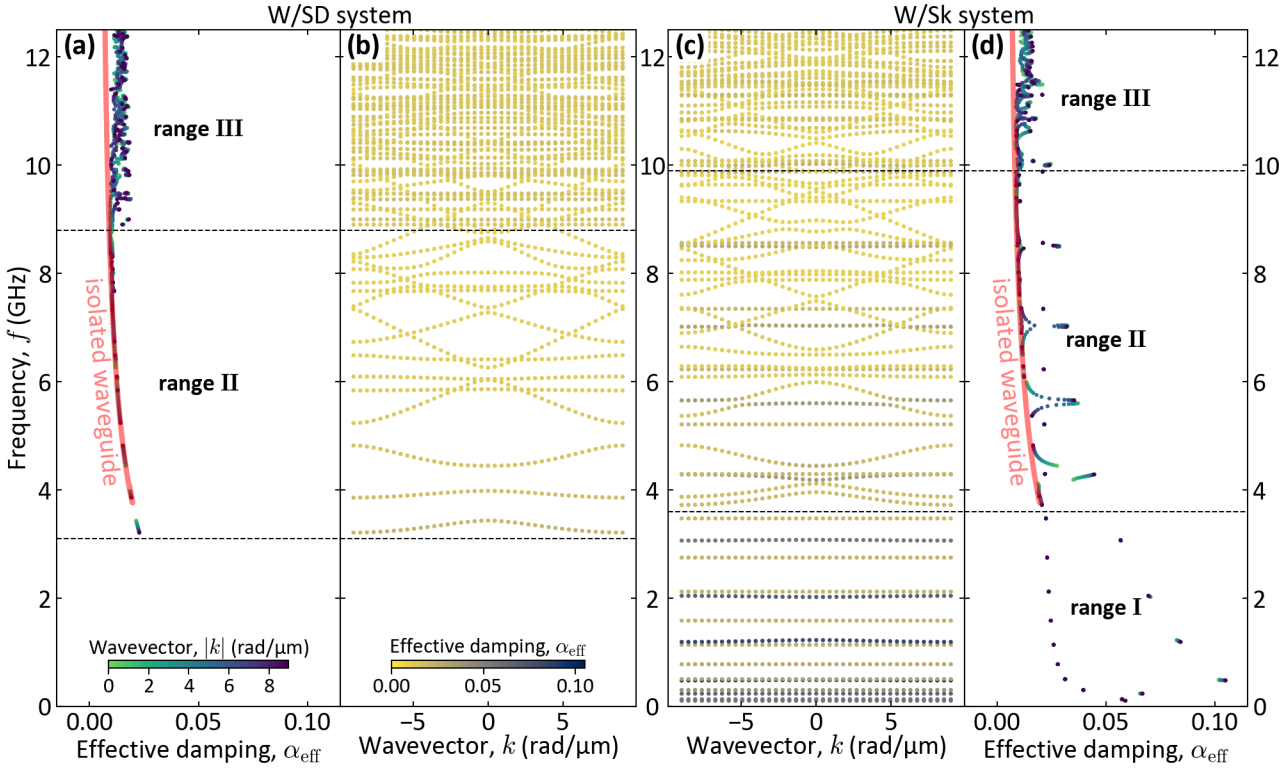

FIG. S3. The dispersion relation in the first Brillouin zone presents effective damping α_{eff} in (b) the W/SD system and (c) W/Sk system. The effective damping of each mode is indicated by the color of the point on the dispersion. The corresponding plots with the effective damping are shown in (a) for the W/SD system and in (d) for the W/Sk system. Here, the color of the point marks the absolute value of the wavevector. Dashed black vertical lines mark the limits of ranges. For the reference, the solid red line in (a) and (d) indicates the effective damping for the isolated waveguide.

are orders of magnitude larger in the W/Sk system. However, it is difficult to distinguish the contribution of modified static configuration of a skyrmion and dynamic dipolar interaction through the waveguide.

S4. IMPACT OF THE DAMPING

In the structures in which the damping varies between subsystems (just as here where the damping of Py waveguide is 0.005 while of the dots is 0.02), the excitation lifetime can give additional information about the system. In the results of the simulations, this information can be found in the frequencies which assume complex values. The ratio of imaginary part to real part of the frequency gives the value of the effective damping $\alpha_{\text{eff}} = \text{Im}(f)/\text{Re}(f)$. This parameter is directly connected with the excitation lifetime since $\mathbf{m}(\mathbf{r},t) = \tilde{\mathbf{m}}(\mathbf{r})e^{i\omega t} = \tilde{\mathbf{m}}(\mathbf{r})e^{i(\omega'+i\omega'')t} = \tilde{\mathbf{m}}(\mathbf{r})e^{i\omega' t}e^{-\omega'' t} = \tilde{\mathbf{m}}(\mathbf{r})e^{i\omega' t}e^{-\alpha_{\text{eff}}\omega' t} = \tilde{\mathbf{m}}(\mathbf{r})e^{i\omega' t}e^{-t/T}$ so $T = 1/\alpha_{\text{eff}}\omega'$. This value depends on the frequency since the contribution of dipolar interactions to the effective damping is nonlinear. It is connected with the Gilbert damping in such a way that $\alpha_{\text{eff}} \geq \alpha$.

The effect of the effective damping on the dispersion relation is shown in Fig. S3. Subfigures (b) and (c) show the dispersion relation for the W/SD system and W/Sk system, respectively, like in Fig. 4(b) and (c) of the main text, but here the color of points marks the value of the effective damping instead of the mode localization. In addition, the value of the effective damping is plotted in subfigures (a) and (d), with the color indicating the wavenumber value from the first Brillouin zone. For reference, the solid red line in (a) and (d) indicates the effective damping for the isolated waveguide.

In the W/SD system, the effective damping is relatively low. In range II, where the modes are localized almost exclusively in the waveguide, the points follow the case of the isolated waveguide. In range III, where the modes are coupled with the dots, the points no longer follow the case of the isolated waveguide, with the effective damping increasing in value. It comes from the fact that due to the coupling with dots, the excitation inside the dot is attenuated faster, effectively decreasing the mode lifetime in whole system.

In the W/Sk system the situation is similar. In range I, the modes are strongly localized in the dots (see, Fig. 4(d) in the main text) and their effective damping is high. The CW modes have higher α_{eff} than CCW modes but the maximum is at the 1st CCW mode. In range II, the modes localized in dots have higher effective damping than modes localized in the waveguide. In the areas where these modes hybridize, the effective damping is gradually changing. This effect resembles the gradual change of the localization shown in Fig. 4(d) in the

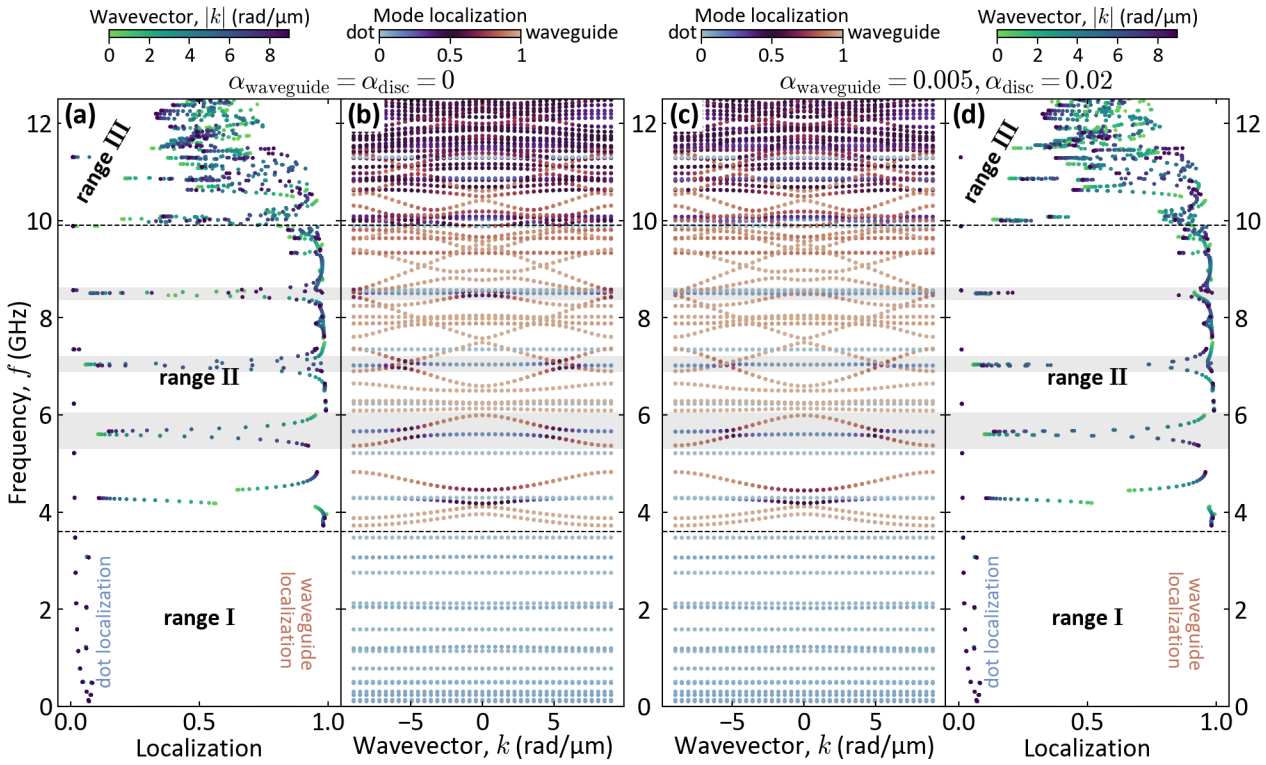

FIG. S4. The dispersion relation in the first Brillouin zone presents the localization of modes in the W/Sk system (b) when the damping is neglected and (c) when it is taken into account. Each mode localization value is indicated by the color of the point on the dispersion. The corresponding plots with the localization value are shown in the case of (a) neglected damping and (d) included damping. Here, the color of the points mark the absolute value of the wavevector. Dashed black vertical lines mark the limits of the characteristic ranges. Gray rectangles indicate the zoom-ins shown in the main manuscript in Fig. 5.

main text. It shows a clear correlation between the mode localization and the effective damping. The situation in range III is analogical to range III in the W/SD system.

In addition to providing information about the mode lifetime, the damping has a significant effect on the spin-wave dynamics, affecting the dispersion relation, especially in the regions of the hybridization between the modes.

Such an effect is shown in Fig. S4. It compares dispersion relations of the W/Sk system in the case of no damping in both subsystems [Fig. S4(b)] with the case of realistic values of damping [Fig. S4(c)]. Most of the modes are not affected by the damping. However, at the hybridizations between the waveguide-dominated and dot-dominated modes, the dispersion of the involved modes can be significantly modulated. We marked three most interesting frequency ranges of dispersion relations with gray rectangles. The discussion about these results is included in the main manuscript in the section "Role of damping on band structure in HMC."

The presented results can raise the question of the possible effect of the hybrid system on the damping if the waveguide were made of a material with lower damping such as yttrium iron garnet (YIG) or CoFeB. The character of the effect on the damping should not change with the material of the waveguide. The dispersion relation should be divisible into ranges analogous to those of the Py waveguide (although the frequency ranges can be shifted) and in each range the effect should be similar. In the W/SD system, in range II, the effective damping should resemble that of an isolated waveguide because the coupling is only static, i.e. it comes from the modified static configuration. In the W/Sk system, in range I, the effective damping should follow the excitation in the CoFeB dot. In range II, the effects of the hybridization between the waveguide and dot modes should be present. In range III, for both systems the effective damping should increase (or decrease if the damping constant of the waveguide is higher than of the dots), compared to an isolated waveguide, which is the result of the strong dynamical coupling of waveguide and dots.